Detection of transient intermediates generated from subsite analogues of [FeFe]-hydrogenases

Neil T. Hunt,[a] Joseph A. Wright*[b] and Christopher Pickett*[b]*

[a] Department of Physics, University of Strathclyde, SUPA, Glasgow G4 0NG, United Kingdom

[b] Energy Materials Laboratory, School of Chemistry, University of East Anglia, Norwich Research Park, Norwich NR4 7TJ, United Kingdom

Abstract

This article reviews the application of transient techniques in the elucidation of electron, proton and photon chemistry related to the catalytic subsite of [FeFe]-hydrogenase from the perspective of research in this area carried out at the UEA and Strathclyde laboratories. The detection of mixed valence states, bridging CO intermediates, paramagnetic hydrides and coordinatively unsaturated species has both informed an understanding of the biological catalysis and stimulated the search for stable analogues of key structural motifs likely involved in turnover states.

Introduction

This Forum article is largely focused on transient FTIR (Fourier transform infrared) techniques that we have used in our laboratories for studying intermediates generated from synthetic analogues of the di-iron subsite of [FeFe]-hydrogenase. This subsite is essentially responsible for the reversible

reduction of protons at the H-cluster of the enzyme. Beyond the enzyme, studies of synthetic di-iron units have provided details of fundamental chemistry important in the wider context of substitution, photoactivation, electron transfer and second coordination sphere interactions. The rich spectroscopy of the enzyme systems themselves has been covered in recent reviews by Lubitz[1] and ourselves.[2]

It is perhaps an overworked tenet of catalysis that if you can isolate a stable intermediate it undoubtedly is not involved in the catalytic pathway. This is the attraction of transient techniques: detecting and identifying energized intermediates provides a blueprint for synthetic modeling of key motifs as stable structurally characterizable compounds.

The catalytic cycle of the [FeFe]-hydrogenase as we presently understand it is represented in Scheme 1.[1,3] This cycle is based upon biochemical evidence and chemical precedent, the underpinning chemistry having been explored over the past 15 years in a variety of chemical models.[4–6] An alternative cycle was proposed recently by King and co-workers who suggested that intramolecular electron transfer to the cluster is concerted with H_2 binding. [7] Some confusion in the representation of the biological system arises from localizing net charges on the cubane, subsite, and in assigning oxidation states to subsite and cluster.

Insight into the reactivity of these small molecule systems is critically-dependent on time-resolved techniques. Physical and chemical processes taking place on timescales from the femtosecond to the second all have vital roles in the production and consumption of protons and electrons. Accessing information about each of these requires application of a range of techniques.

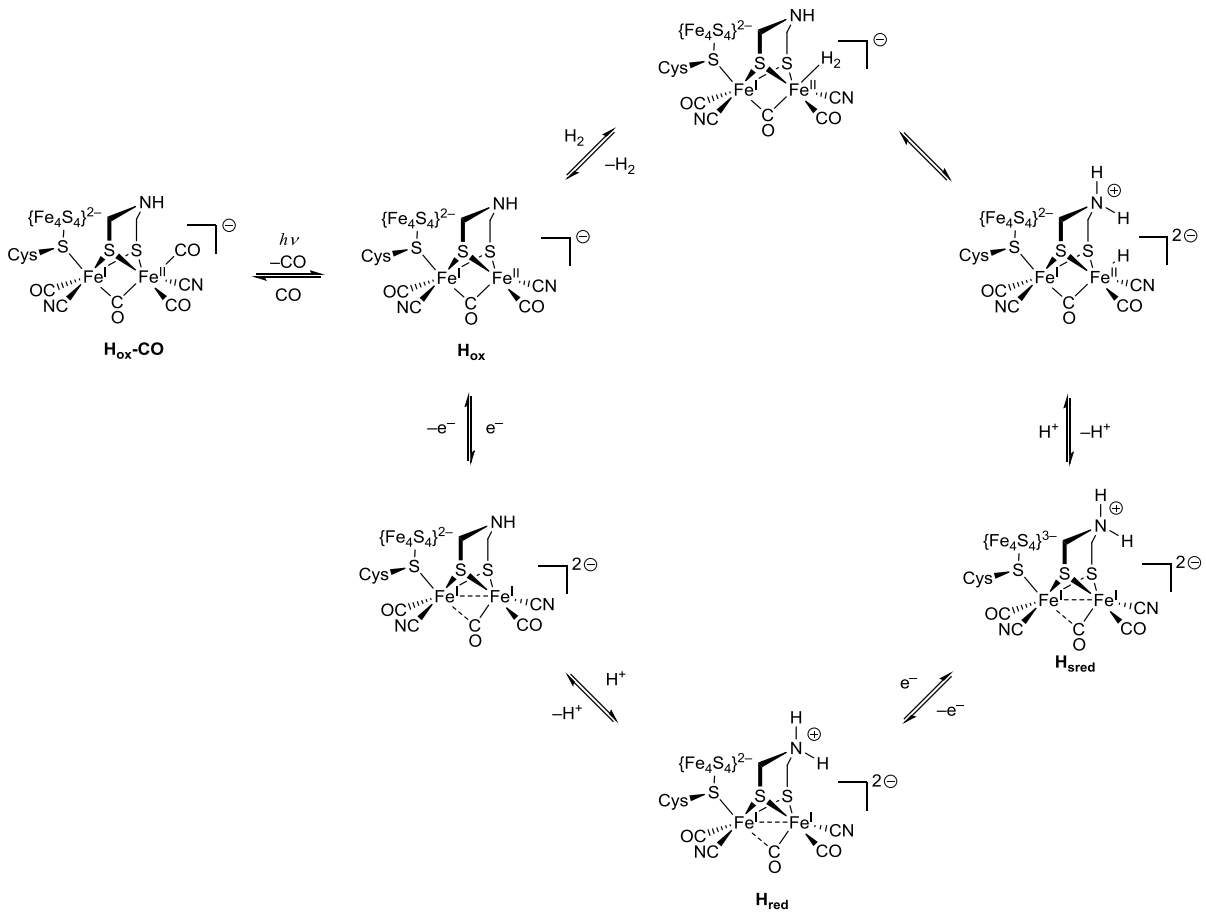

Scheme 1. Catalytic cycle for [FeFe]-hydrogenase; the $\{Fe_4S_4\}$ cluster is ligated by three additional cysteinyl residues; the charge adjacent to the partial bracket is the net charge on the subsite unit; the charge on the bridging amine is localized.[1,3,6] See ref. 7 for an alternative formulation.

Laser (pump-probe) spectroscopies offer insight into the fastest physical variations in the models, in particular solvation of activated complexes and the communication between bonds (vibrational modes). Solvent-adduct species related to the [FeFe]-hydrogenase have been detected under these conditions.[8]

The fastest chemical processes detected for model complexes take place on the timescale of microseconds to milliseconds. Here, stopped-flow spectroscopies may be applied: rapid mixing of reagents and detection by either ultraviolet-visible (UV-vis) or infrared (IR) methods can be used to study these rapid changes. Evidence for short-lived intermediates in the protonation of electron-rich

species, along with kinetic data on rapid reactions, has given new insight into the formation of hydrides.[9,10]

Electrochemistry offers a unique viewpoint into species with lifetimes of seconds or less, and when combined with rapid spectroscopies this can be a particularly powerful approach to probing electron transfer chemistry. Evidence for both bridging Fe(I)Fe(II) carbonyl species[11,12] and for mixed-valence bridging hydrides[13] has been accessed in this way.

In concert with these efforts to characterize transient species, significant progress has been made in finding routes to isolable analogues of unstable species. Modification of the coordination environment about the metals is a powerful approach to forming stable analogues of species known only from spectroscopic data. Thus insight into the nature of reactive complexes has helped to drive synthetic effort, which provides isolable compounds for which structural parameters may be determined.

Stopped-flow studies of protonation and substitution

As shown in Scheme 1, protonation of the natural system is believed to take place in a terminal manner, with the bridging position in the enzyme occupied by a carbonyl group (the so-called rotated state).[3,6] Protonation studies in model systems have focused on electron-rich models featuring one or more phosphine ligands on {2Fe2S} or {2Fe3S} cores (Figure 1);[14–18] protonation of cyanide-containing derivatives has been much less extensively studied due reactions of ligand itself under the same conditions (vide infra).[15,19]

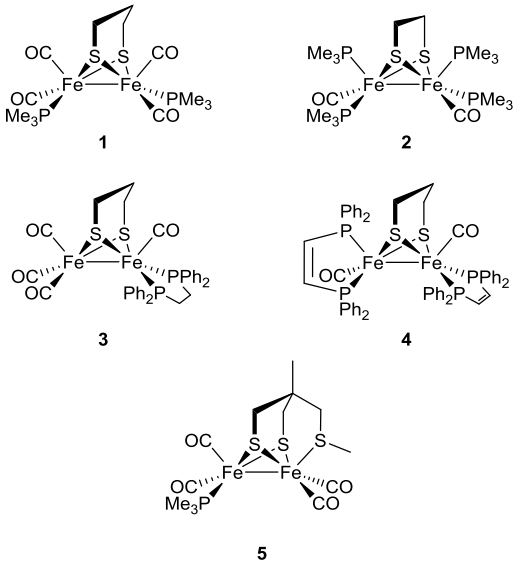

Figure 1. Examples of protonatable model complexes.[14–18]

The first protonation study of **1**[14] established the formation of bridging hydride as the isolable reaction product at room temperature. Subsequent studies on a wide range of systems have demonstrated that this is the thermodynamic outcome: terminal hydrides, if observed, will isomerize to bridging hydrides. In 2005, Rauchfuss and co-workers were able to isolate a terminal hydride by *reduction* of a highly-oxidized system using the hydride source AlH_4^- (**6**, Figure 2).[20] The first experimental evidence for the existence of terminal hydrides formed by *protonation* of a neutral precursor was reported by Schollhammer and co-workers in a low-temperature nuclear magnetic resonance (NMR) study.[16] At 203 K, protonation of **3** gives a single signal in the hydride region at −4.33 ppm, which on warming to room temperature is converted to a triplet at −14.23 ppm (J_{HP} = 21 Hz). The lack of coupling between the hydride and phosphorus was interpreted as indicating that the terminal hydride is in the apical position (Figure 2), an effect observed in other NMR protonation studies (see below).

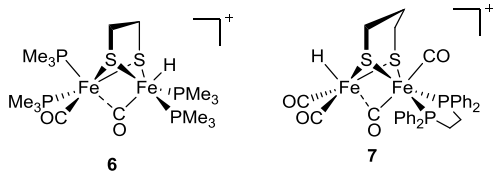

Figure 2. First crystallographically- and spectroscopically-characterized terminal hydrides.[16,20]

A key question is the pathway by which protonation occurs: is reaction at the bridging position preceded by formation of an observable terminal species? Stopped-flow (SF) studies offer one way to gain insight into this process. In the stopped-flow experiment, two solutions are mixed rapidly in a microfluidic chamber (typically with a mixing time below 20 ms). The solution is then allowed to flow into a spectroscopic cell, where observations can be made in the UV-vis (SF-UV) or the infrared (SF-IR). Practical considerations and the nature of the detection methods lead to some differences in the physical set up for these two approaches, but conceptually the outcomes are the same: time-resolved spectroscopic data for a reaction with temporal resolution far beyond that which can be obtained by other means.

Using a combination of SF-UV and SF-IR, we have been able to establish a clear picture in the protonation pathways for a wide range of {2Fe2S} and {2Fe3S} models.[9,10,18,21] For systems of general formula $Fe_2(xdt)(CO)_4(PMe_3)_2$ (xdt = alkyl-α,ω-dithiolate), protonation on the metal−metal bond takes place rapidly, on the order of milliseconds for the fastest reactions. This process can be followed by loss of metal−metal bonding character, which results in depletion of the characteristic UV-vis band at ∼355 nm (Figure 3). In all cases, the loss of intensity may be modelled as a single exponential decay, consistent with pseudo-first order kinetics under excess acid conditions.

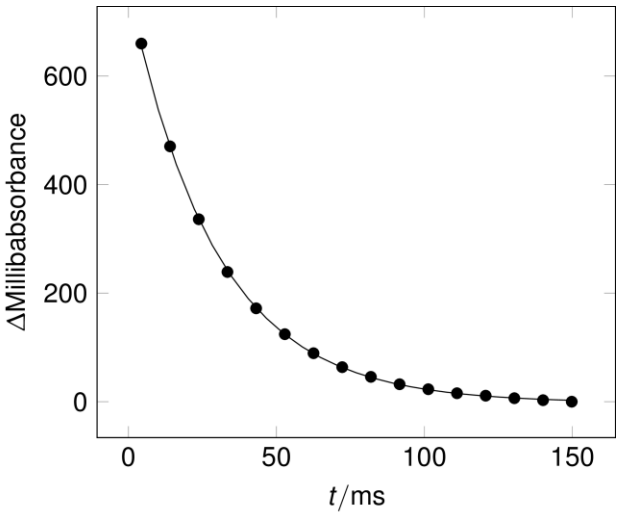

Figure 3. Example time course for loss of metal–metal bond signal in **1** on protonation by $HBF_4{\cdot}Et_2O$ in MeCN (adapted from ref. 9 with permission from the Royal Society of Chemistry). (Points: experimental data; line: exponential fit.)

Whilst SF-UV confirms that protonation is a rapid single-step process, it cannot give direct evidence for the site(s) of protonation. The rate data from these experiments may be compared with that obtained under identical conditions in the SF-IR, confirming that the loss of the UV signal occurs in concert with appearance of IR bands for bridging protonated products (Figure 4, Figure 5). This clearly shows that there are two distinct phases to the reaction: a rapid first step leading to a large shift ($\sim$100 cm^{-1}) in the average peak position (Figure 4, left), and a second slower phase in which the change of peak position is much more subtle (Figure 4, right). Notably, the first phase of the reaction also leads to a change of peak pattern, from four bands (two overlapping) to two bands. The second phase only involves a displacement of these intermediate bands.

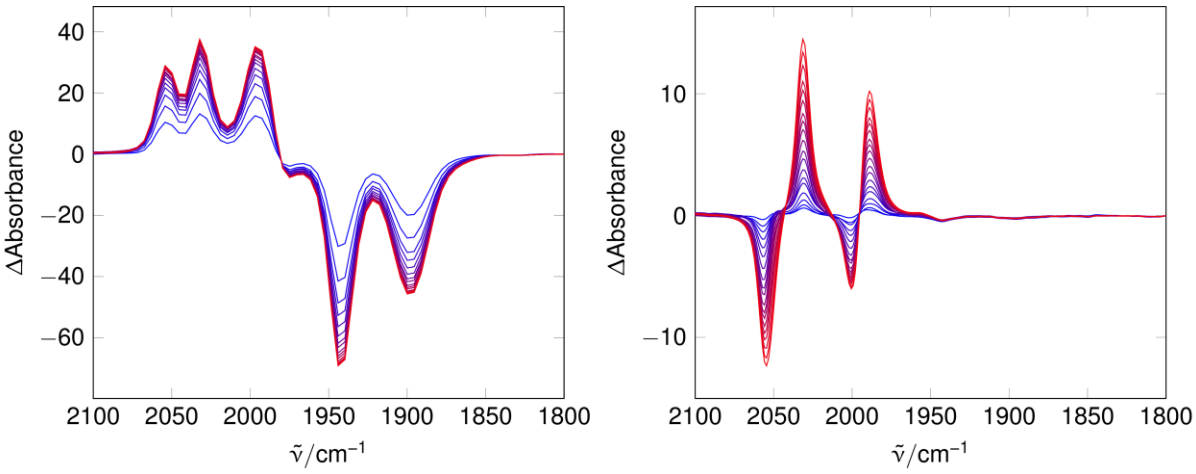

Figure 4. Example IR difference spectra for protonation **1** by $HBF_4{\cdot}Et_2O$ in MeCN (adapted from ref. 9 with permission from the Royal Society of Chemistry). Left: short time (70 ms to 780 ms); Right: long time (1 s to 162 s). Time runs from blue to red in both cases.

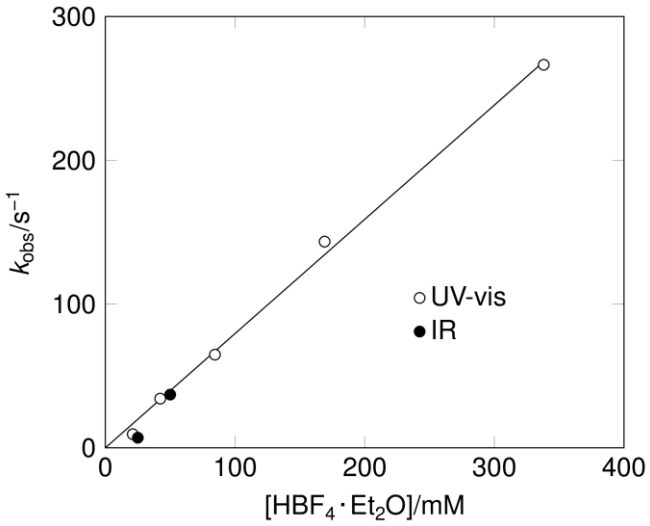

Figure 5. Comparison of rates of **1** by $HBF_4{\cdot}Et_2O$ in MeCN (adapted from ref. 9 with permission from the Royal Society of Chemistry).

The protonation reaction is deceptively simple. Reaction of the trans-dibasal parent with acid leads ultimately to the trans-dibasal protonated product (Scheme 2). However, the major product of the initial protonation reaction is the apical-basal isomer. This is explained by rotation of the ligand set at one iron center to allow access of the solvated proton at one side of the metal−metal bond, a mechanism supported by density functional theory (DFT) transition-state calculations.[22]

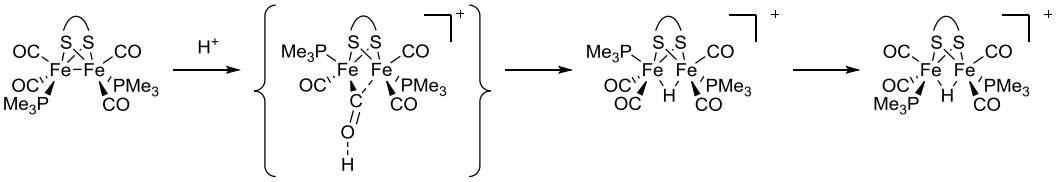

Scheme 2. Dominant protonation pathway for {2Fe2S} systems including postulated transition state for primary protonation.[10,22]

Although the protonation reactions studied are in general too fast to examine completely by NMR, it is possible to gain some insight into the process by using a suitable set of conditions. Using this approach, we were able to confirm the presence of distinct bridging hydrides, with protonation of **1** giving three signals in the hydride region of the ^{1}H spectrum (ca −15 δ). The multiplicity of these signals could be used to confirm the nature of the species involved, with the apical-basal isomer yielding a doublet whilst the two basal-basal variants both exhibit triplets.

Whilst the general pattern of behavior is similar for all of the complexes $Fe_2(xdt)(CO)_4(PMe_3)_2$, the kinetic analysis reveals important detail not visible from other data. The first hints of this were obtained when we examined protonation of the ethane-1,2-dithiolate (edt) bridged species **8** (Figure 6).[10] Despite the close structural analogy to **1**, the rates of both initial protonation and the subsequent rearrangement are around ten times as slow in **8**. Intrigued by this result, we examined the protonation rates of a series of mono- and bis-phosphine complexes with a variety of alkyl bridges (Figure 7).[21] Increasing the steric bulk of the dithiolate group does not significantly disturb the IR stretching frequencies observed, with the least reactive (edt) and most reactive (iPr$_2$-pdt) both having carbonyl bands falling in the same 1980−1898 cm^{-1} region. However, the difference in reactivity can readily be accounted for by consideration of the oxidation potentials of the parent, unprotonated species.

The orbital character of the HOMO (highest occupied molecular orbital) corresponds closely to the 'bent' Fe–Fe bond in these di-iron systems. Thus, both the protonation of the metal–metal bond and oxidation of the di-iron complexes engages the HOMO directly. For a reversible one-electron

oxidation process in solution, the value of $E_{1/2}$ can be viewed as a relative measure of the energy of the HOMO, provided the solvation energy differences between oxidized and reduced forms are very similar or vary systematically.[23] There is a clear linear free energy relationship between ln k_H and $E_{1/2}$

$$\ln k_{\mathrm{H}} = \frac{F(c - \beta E_{1/2})}{RT} \tag{1}$$

where β is the Brønsted coefficient and c is a constant which depends on the chosen reference system. Inserting these values and those for known constants at room temperature leads to the simplfied form

$$\log k_{\mathrm{H}} = 0.20 - 11.7E_{1/2} \tag{2}$$

A fast pre-equilibrium would shift the redox potential of the dialkyl bridgehead substituted species negative towards that of the more easily oxidized semi-bridged species, conserving the general correlation between ln k_H, $E_{1/2}$ and the energy of the HOMO (Scheme 3). Bulkier alkyls displace the equilibrium toward the semi-bridging form, both favoring protonation and reducing the oxidation potential.

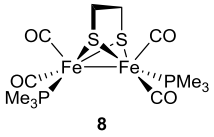

8

Figure 6 Ethane-1,2-dithiolate bridged model.

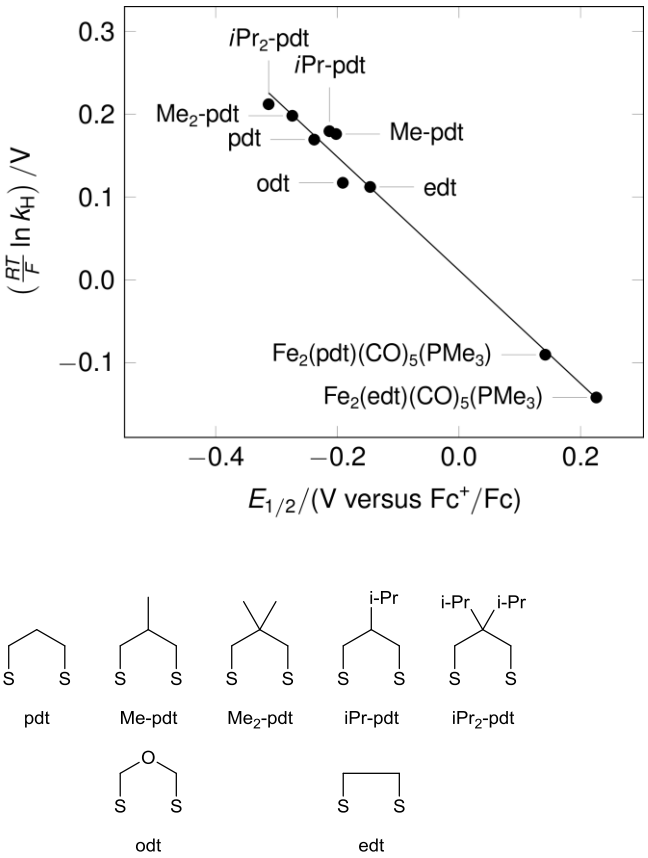

Figure 7. Variation of protonation rate with oxidation potential (adapted from ref. 21). Complexes are of the form $Fe_2(xdt)(CO)_4(PMe_3)_2$ unless otherwise specified. Bridges: adt = 2-azapropane-1,3-dithiolate, odt = 2-oxapropane-1,3-dithiolate, Me-pdt = 2-methylpropane-1,3-dithiolate, Me_2-pdt = 2,2-dimethylpropane-1,3-dithiolate, *i*Pr-pdt = 2-isopropylpropane-1,3-dithiolate, *i*Pr_2-pdt = 2,2-bis(isopropyl)propane-1,3-dithiolate. Fc = ferrocene, Fc^+ = ferrocenium.

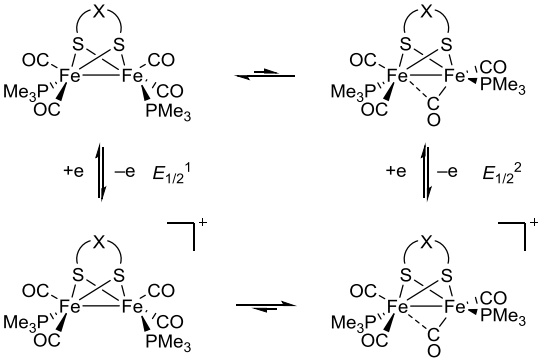

Scheme 3. Equilibrium scheme-of-squares accounting for influence of dithiolate steric bulk on oxidation potential and thus protonation rate.[21]

This relationship holds not only when considering the steric influence of the dithiolate ligand on reaction rate but also the electron-donicity of the core ligand set. Protonation of {2Fe3S} assemblies viz. **5** proceeds to give the first bridging hydride of this type of core with a protonation rate broadly in accord with the correlation observed.[18] Monophosphine {2Fe2S} complexes show both a much lower rate of protonation and much increased oxidation potential, and this variation may be modelled as part of the same linear free energy relationship. Thus it is possible to estimate the rates for bridging protonation in species which cannot be measured experimentally, with the proviso that this assumes no change of mechanism for what may be disparate reaction conditions. In particular, the protonation rate for the enzyme active site itself may be estimated: given the reported oxidation potential for the natural system (−420 mV versus SHE) the estimated rate of bridging protonation at pH 7 is roughly 10^5 s^{-1}, a value in line with the observed turnover rate for the enzyme and thus suggesting that metal protonation is not the rate-limiting step in the reaction.[24] (Note that in the original publication this value is erroneously given as 10^3 s^{-1}.)

Notably, all of the systems explored by us have shown no evidence for any intermediates featuring terminal hydrides detectable on millisecond timescale at ambient temperature. Whilst terminal species have been detected in the NMR at low temperature given an appropriate ligand framework, there is strong evidence that they are *not* precursors to the formation of the bridging hydrides (i.e. the two are formed in separate competing pathways).[15] However, terminal hydrides do rearrange to the bridging structures. At low temperatures the rate of formation of a bridging hydride can be at least as fast as that of a terminal hydride. This has been taken to indicate that terminal hydrides are not on the direct pathway to bridging hydrides, although they will rearrange to the thermodynamic bridging hydride over time. Thus the intermediary of transient terminal species in the formation of bridging hydrides is currently only supported by computational simulation.[22]

As noted earlier, studying the protonation of cyanide-containing systems such as **9** (Scheme 4) is complicated by decomposition of the complexes in the presence of excess acid. Protonation at

cyanide also significantly retards the rate of protonation at the metal center (the thermodynamic product of reaction with acid),[19] but this can be observed at equimolar acid concentration.[14,25] Independently, it is possible to estimate the rate of reaction one would expect for direct protonation of the metal-metal bond based on the relationship to oxidation potential detailed above.[21] This yields a value for the second-order rate constant of around 9×10^5 M^{-1} s^{-1} based on the reported $E_{1/2}$ (−0.49 V vs Fc^+/Fc[26]).

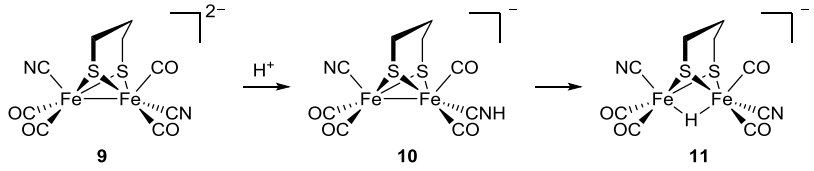

Scheme 4. Protonation of cyanide-containing model.[25]

A similar pattern of kinetic protonation at nitrogen followed by slower transfer to the thermodynamically-favored metal-bridging site has been seen using in situ IR methods by Lomoth and co-workers in studies of complex **12** (Figure 8).[27] Again, using the linear free energy relationship between protonation rate and oxidation potential, it is possible to estimate that the rate of direct protonation at the metal would be similar to that for **1** (i.e. that the remote base neither aids nor hinders reaction).

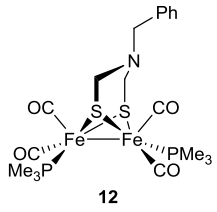

Figure 8. Substituted azadithiolate examined by Lomoth and coworkers.[27]

As well as protonation, SF-IR has been used to examine the detailed substitution mechanism in the conversion of **13** to **17** under conditions of excess cyanide (Scheme 5).[11] This study demonstrated addition of the first cyanide ligand is fast but that direct introduction of the second is slow and occurs only under relatively forcing conditions. Instead, the more favorable route to **17** is to react via

a thioether off-on-off mechanism. Importantly, this involves the formation of bridging CO species with labelling studies showing that attack by CN^- at one iron leads to CO transfer to the other (**TS-13-14**). Kinetics in the substitution of the prototypical model **18** (Figure 9) have also been investigated by Darensbourg and co-workers using in situ IR methods,[28,29] revealing the pathways by which both cyanide and phosphine groups are introduced into these units.

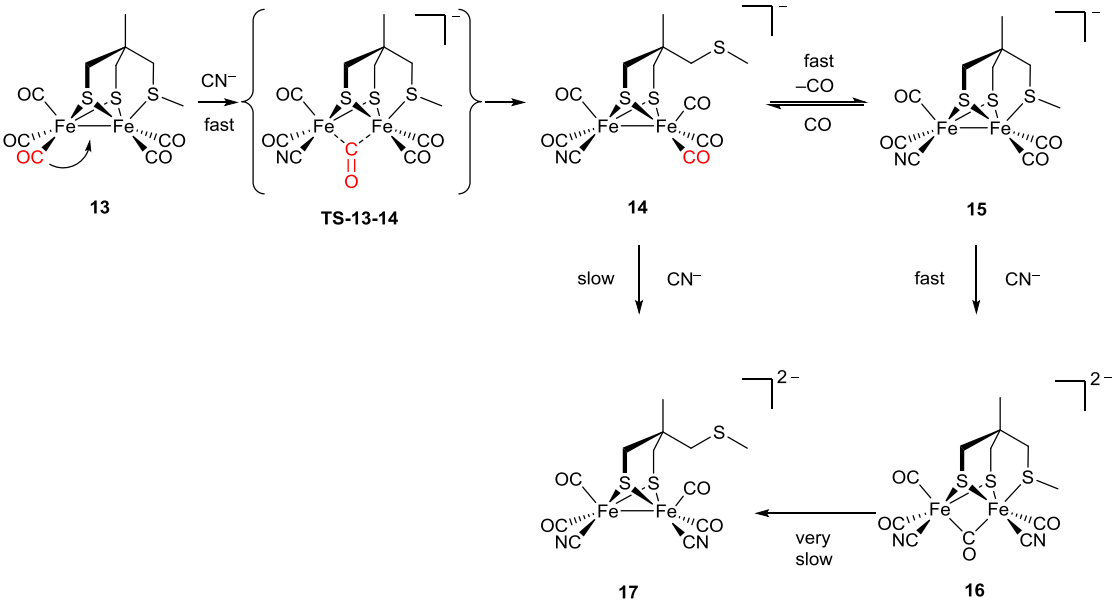

Scheme 5. Role of bridging CO in cyanide substitution at {2Fe3S} centers (adapted from ref. 11 with permission from the Royal Society of Chemistry).

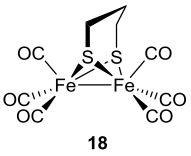

Figure 9. Prototypical [FeFe]-subsite unit model.

Structural analogues of the enzyme have been reported which feature either a {4Fe4S} cubane[30] or a surrogate of similar redox potential,[31–33] and the latter engage in (slow) hydrogen oxidation catalysis. However, whilst this group is doubtless important not only in the electron transfer, but also in tuning the stereoelectronic properties of the catalytic site, to date transient studies involving redox-

appended subsite models have been largely limited to photoreduction involving Ru(II) chromophores or related antennae (see below).

Spectroelectrochemistry of transient intermediates

In the resting state of the enzyme the subsite is a mixed-valence Fe(I)Fe(II) unit with a (semi)bridging CO and an apical site vacant or coordinated by water.[3,6] FTIR spectroelectrochemistry or stopped-flow FTIR using ferrocenium as an oxidation showed that the dicyanide complex **19** (Scheme 6) with an appended thioether group underwent single one-electron oxidation to give an unstable paramagnetic Fe(I)Fe(II) mixed valence species with a {2Fe3S} core.[11] This spin-half species provided the first chemical evidence for the resting state structure in the enzyme. More recently, Ott, Lubitz and co-workers showed the corresponding generation of mixed-valence systems using a related species with functionalize azapropanedithiolate ligand.[34] Seminal work by Darensbourg showed that replacement of cyanide by an N-heterocyclic carbene allowed the isolation and structural characterization of stable mixed-valence systems,[35] whilst Rauchfuss and co-workers showed that Fe(I)Fe(II) species with semibridging CO could be stabilized as structurally-characterizable species using the rigid dppv [1,2-bis(diphenylphosphino)ethane] ligand.[36]

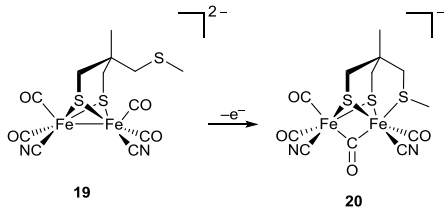

19 **20**

Scheme 6 Transient formation of a mixed-valence Fe(I)Fe(II) state with a bridging CO.[11]

Studies of the electron transfer chemistry of synthetic di-iron units and of their ability to electrocatalyze proton reduction or dihydrogen oxidation intrinsically underpin understanding of model systems. These have been extensively reviewed; that of Gloaguen and Rauchfuss is particularly accessible.[5] FTIR spectroelectrochemical studies have provided much useful information on reactive intermediates associated with reduction, oxidation and electrocatalysis. An early study of

the prototypical subsite model **18** showed that the primary electron transfer event was a partially-reversible one-electron reduction followed by chemistry involving decoordination of one thiolate, further electron transfer and attack on a parent molecule to give a tetrairon assembly.[37] Formation of the latter was deduced by EXAFS (extended X-ray absorption fine structure) using a novel continuous flow system designed by Dr Stephen Best. Full support for this interpretation of the EXAFS data came from a synthetic study by Heinekey, who isolated a tetrairon unit (Figure 10).[38] The hexacarbonyl system was also shown to be an moderate catalyst for proton reduction with respect to turnover but a poor catalyst with respect to overpotential.[37]

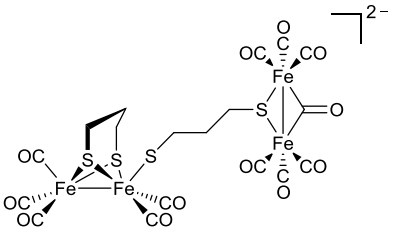

21

Figure 10. Tetrairon system isolated by Heinekey and co-workers.[38]

It is clear that catalysis is only effected by accessing the Fe(I)Fe(0) state of the di-iron unit, as is the case with other analogues, whereas the natural system almost certainly turnover occurs at the Fe(I)Fe(II)/Fe(I)Fe(I) level. Of rather more relevance to the natural system is the behavior of the tetrairon assembly shown in Scheme 7 which can be considered as two fused di-iron units with formal oxidation states Fe(I)Fe(II).[39–41] This complex electrocatalyzes proton reduction at the Fe(I)Fe(I) level via the formation of a bridging carbonyl intermediate. Importantly, formation of the catalytic intermediate following electron transfer involves the exposure of a coordination site at iron by rearrangement of a terminal to a bridging CO. Spectroelectrochemical studies clearly demonstrated the generation of the bridging CO intermediate in the absence of a proton source, with DFT calculations supporting the structure proposed.[42] Electrocatalysis of proton reduction is ca 500 times faster than from the monomeric **18**. The dramatically increased rate obtained for the dimeric system over all previously-identified model compounds appears to be related to the features

uniquely-common between it and the H-cluster, namely turnover involves the same formal oxidation states of the di-iron unit and the thiolate bridge to a second one-electron redox unit.

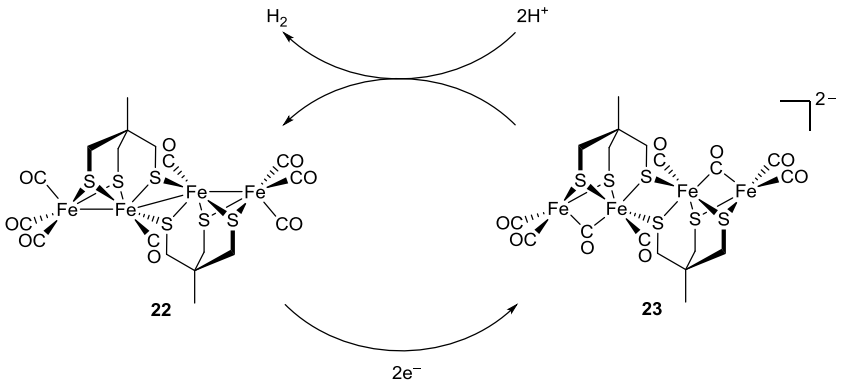

Scheme 7. Dimeric {4Fe4S} system electrocatalyzing proton reduction at the Fe(I)Fe(I) level.[39]

Fe(II)Fe(II) hydrido species in which the proton occupies a bridging or terminal position are likely intermediates in electrocatalysis, with the terminal hydrides most probably associated with the natural system (Scheme 1). Closed-shell bridging hydrides of the type shown in Figure 11 can undergo one electron reduction to give reactive intermediates (Figure 12). FTIR spectroelectrochemical studies and low-temperature EPR (electron paramagnetic resonance) studies have established that one-electron transfer does not lead to major structural rearrangement, and that the 'additional' electron is delocalized across the di-iron system.[13,18] This interpretation was later supported by Rauchfuss and co-workers, who showed that with suitably substitution of the core a delocalized 35-electron species could be isolated and structurally characterized (Figure 13).[43]

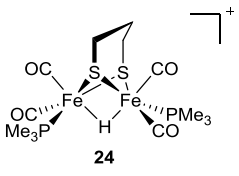

Figure 11. Bridging hydride structure.

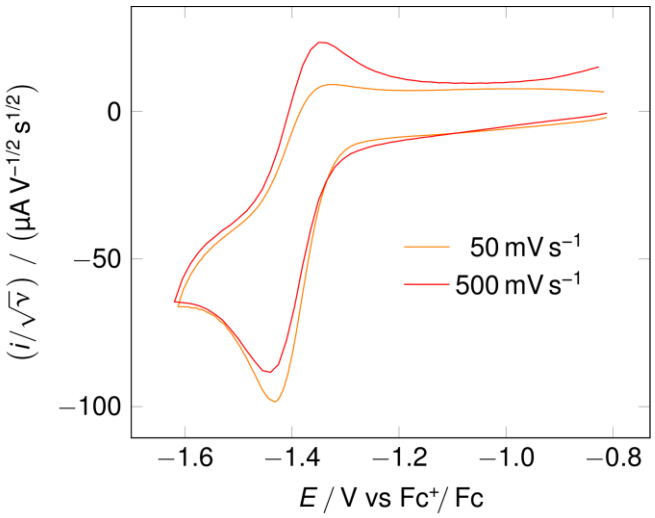

Figure 12. Normalized cyclic voltammograms of **21** (10 mM) recorded at a vitreous carbon working electrode in 0.1 M $[Bu_4N][BF_4]$-MeCN at 25 °C. (Reprinted with permission from ref. 13. Copyright 2008 American Chemical Society.)

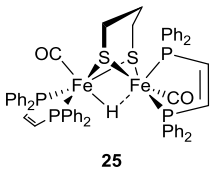

25

Figure 13. Structurally-characterized 35-electron hydride reported by Rauchfuss and co-workers.[43]

The instability of the 35-electron systems is associated with ligand dissociation, PMe_3 or intramolecularly-bound thioether, to give a 33-electron system, which is further reduced to a closed-shell monoanion.[18] FTIR spectroelectrochemistry combined with DFT studies provided evidence for the formation of these unprecedented Fe(I)Fe(I) bridging hydrides, in which a coordination vacancy is asymmetrically exposed at one of the iron sites (Scheme 8). Support for the existence of this super-reduced bridging hydride state comes from the observation that a 'trapped' bridging hydride/terminal hydride species is synthetically-accessible, again using the rigid dppv ligand framework,[44] with the bridging hydride functioning as a spectator ligand for hydrogen evolution upon further protonation.[43]

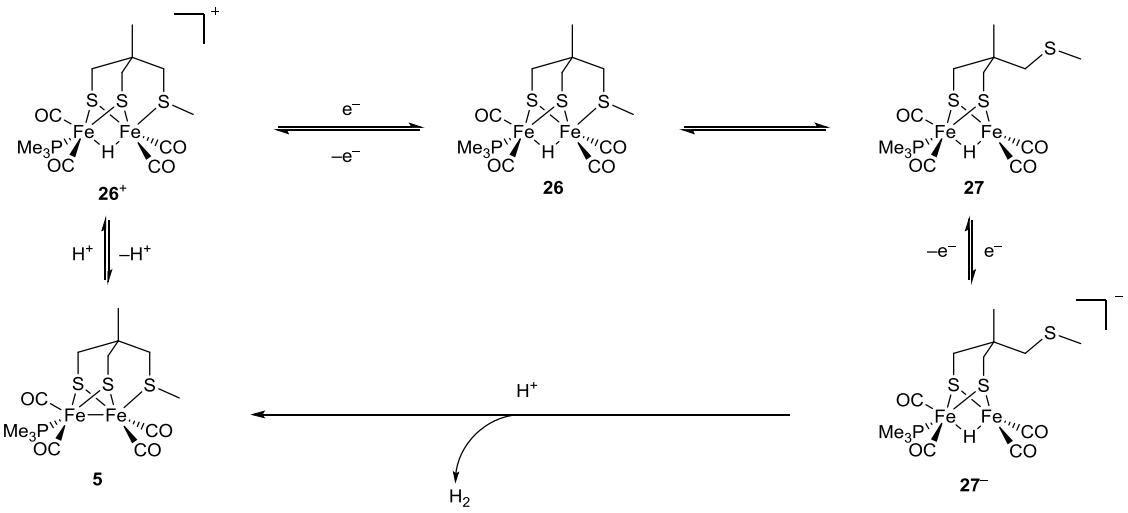

Scheme 8. Formation and behavior of the super-reduced state.[18]

Photochemistry and physics

A number of studies have been undertaken using ultrafast time-resolved spectroscopy methods to interrogate hydrogenase sub-site analogues. These fall into two categories. The first features two-dimensional infrared (2D-IR) spectroscopy investigations of the ground state structure, vibrational relaxation and solvent interaction dynamics while the second seeks to determine the response of sub-site analogues to light-activation in order to provide insights into the resulting reaction mechanisms. In both cases the work to date has concentrated mainly upon di-iron hydrogenase-inspired systems.

Ground state structure, solvation and dynamics

The first application of 2D-IR spectroscopy to hydrogenase analogues reported the electronic ground state structure and vibrational dynamics of **18** in heptane solution (Figure 14).[8] By comparing 2D-IR spectra of **18** with density functional theory calculations, it was determined that the structure of the molecule in solution was similar to reported crystal structures and in good agreement with gas-phase simulations. The presence of off-diagonal peaks in the 2D-IR spectra showed that the carbonyl stretching vibrations were coupled across the whole molecule as opposed to within $Fe(CO)_3$ substructures. Experiments to determine the vibrational relaxation dynamics of this molecule revealed a solvent-dependent few-picosecond equilibration of energy between the carbonyl

stretching modes, assigned to intramolecular vibrational energy redistribution (IVR), accompanied by a slower (~100 ps) relaxation process to the vibrational ground state.

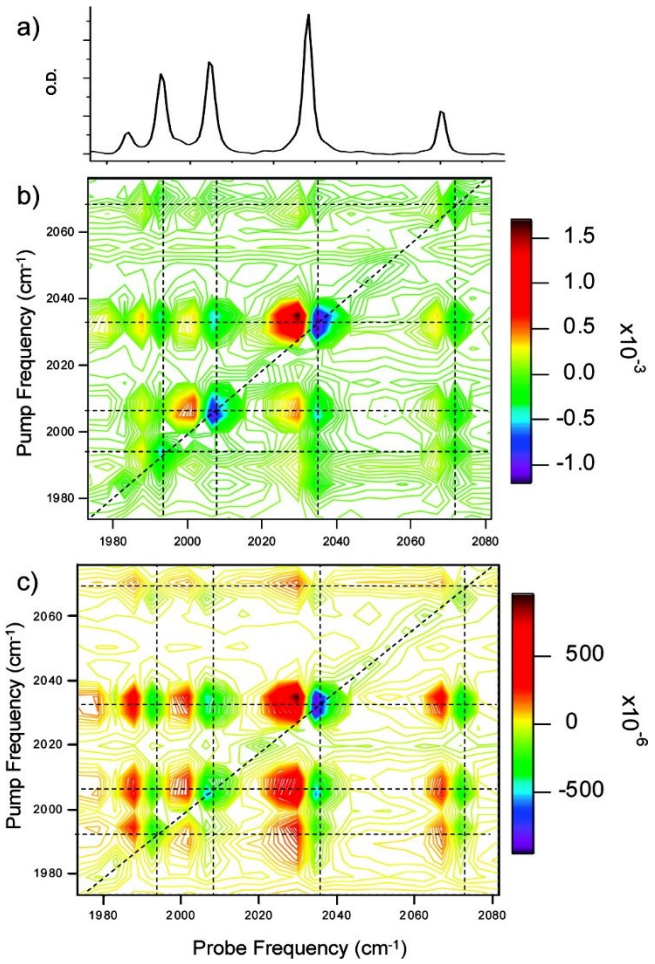

Figure 14. (a) FTIR spectrum of a 1 mM solution of **18** dissolved in heptane. (b) 2D-IR spectrum of the same sample with a pump−probe time delay of 5 ps. (c) As with b, but with a pump−probe time delay of 25 ps. (Reprinted with permission from ref. 8. Copyright 2008 American Chemical Society.)

The impact of exchanging CO for CN ligands and so mimicking more closely the enzymatic active site, was subsequently investigated using 2D-IR spectroscopy to probe the vibrational dynamics of **9** (Scheme 4).[44] The results indicated that, in contrast to the CO modes discussed in the initial publication, the vibrational coupling between the stretching modes of the CO and CN ligands is small and restricted to certain modes. Additionally, slow growth of off-diagonal peaks was observed and assigned to population transfer processes occurring between CO and CN modes on timescales of 30–40 ps; significantly slower than the inter-CO mode IVR process. Analysis of the dynamics in concert

with anharmonic density functional theory simulations showed that the presence of CN ligands altered the vibrational relaxation dynamics of the CO modes in comparison to all-carbonyl model systems and suggested that the presence of these ligands in the enzyme may be an important feature in terms of directing the vibrational relaxation mechanism. Vibrational relaxation plays an important role in energy dissipation following the formation of non-equilibrium structures during a reaction. As such, information on the routes through which molecules dissipate energy provides useful insight into the roles of elements within the molecular structure. This is particularly important in complex species such as enzymes.

The interaction of the subsite analogue with its surroundings, either the protein scaffold in the enzyme or the solvent in a synthetic system is likely to be important in determining or controlling behavior.[46] Ultrafast 2D-IR spectroscopy was utilized to study the structure and solvation dynamics of **28** (Figure 15) in solvents ranging from non-polar to polar and protic. In this case the temporal dependence of the 2D-IR lineshape was used to extract information relating to hydrogen bond-related dynamics of the carbonyl modes in protic solvents via a phenomenon referred to as spectral diffusion. The influence of the solvent bath on vibrational relaxation, including rapid intramolecular population transfer, was also characterized and comparisons with previous 2D-IR studies were used to deliver insights into the dependence of the rate of population transfer upon vibrational mode separation and solvent environment.

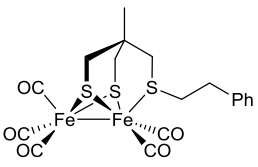

28

Figure 15. Tripodal model.

Excited state photochemistry and dynamics

Several studies have been made using UV-wavelength light to activate photochemistry of hydrogenase subsite analogues, and indeed the enzymes themselves. These were generally steady state measurements carried out under constant illumination and provided important insights into the impact of light on these species and the potential for photochemical control. In order to elucidate the underlying molecular mechanisms of photoactivation, we performed a sequence of studies employing ultrafast excitation at UV wavelengths followed by IR-probing of the ensuing chemistry.

The first such measurement investigated the **18** species (Scheme 8).[47] By combining ultrafast UV-pump infrared (IR)-probe spectroscopy, steady-state Fourier transform-IR spectroscopic methods, and density functional theory simulations, it was determined that irradiation in an alkane solution at 350 nm led to the formation of a 32-electron complex **29** caused by loss of a carbonyl ligand within 50 ps with evidence of a weakly associated solvent adduct complex (Figure 16). Full recovery of the initial complex was found to take place on timescales covering several minutes.

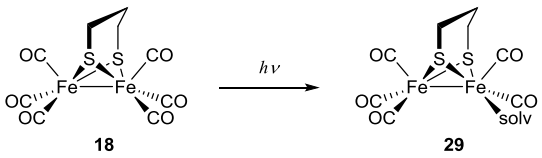

18 29

Scheme 8. Formation of solvato-species after irradiation.

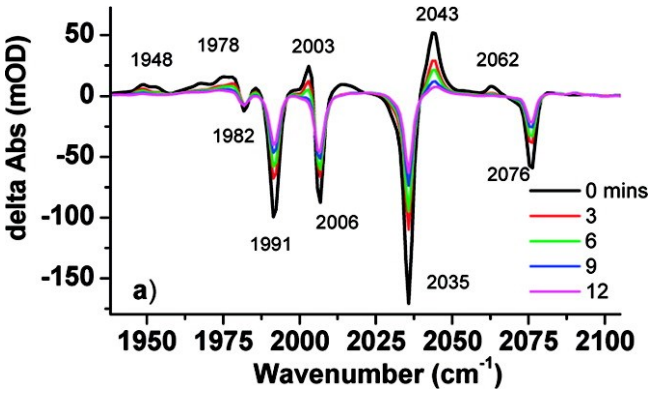

Figure 18. Steady-state UV−FTIR difference spectrum of **18** in heptane at a range of times following 60 s UV irradiation. (Reprinted with permission from ref. 47. Copyright 2008 American Chemical Society.)

The evidence for UV radiation creating a vacant coordination site was consistent with other studies of organometallic carbonyl systems,[48,49] while the maintenance of a metastable weakly-bound solvent adduct provided the possibility for light-activated chemistry. Similar observations were also well-known from studies on the enzymes themselves with various experimental methods revealing the photo-lability of CO ligands that were able to inhibit H-cluster function.[50–61]

The ultrafast work reported in ref. 47 was subsequently extended by a study of the same system but over a wider range of time scales.[62] In this case, nanosecond time-resolved infrared spectroscopy was used to fill in some of the temporal gaps between the femtosecond−picosecond experiments and steady-state UV-FTIR methods used in the first publication while additional solvents (heptane, acetonitrile and cyanoheptane) were investigated. Once again, the rapid (sub-ps) formation of solvent adduct species from the first solvation shell of the solute following photolysis of a carbonyl ligand was observed and global fitting techniques provided insights into the ultrafast dynamics of this process, showing CO loss to be near-instantaneous. Most relevantly for mechanistic studies, the use of solvent mixtures and longer timescale experiments enabled the observation of competitive, diffusive ligand substitution processes at the newly created coordination site on time scales of a few nanoseconds, shedding new light on the chemical behavior of these enzyme models.

This molecule has been subsequently studied by others using similar methods but including excitation at longer wavelengths. A relative insensitivity to wavelength was reported although it was suggested that some spectral influence due to Fe−Fe bond lengthening was present under longer wavelength excitation conditions.[63]

A question arising from the initial study of the photochemistry of this species was whether a single CO-loss isomer was formed or a mixture. To investigate this further, ultrafast transient 2D-IR (T-2D-IR)

spectroscopy was used to probe the photolysis products in more detail.[64] By observing coupling patterns between the vibrational modes of the photoproduct species as well as examining the appearance time scales of these signals we were able to assign the photoproduct spectrum to a single pentacarbonyl species. Comparison of the vibrational relaxation rate of the photoproduct with that of the parent showed faster relaxation rates for the new species and this was attributed to the formation of a solvent adduct at the vacant coordination site.

The inclusion of non-carbonyl ligands into subsite analogues has been shown to be beneficial in terms of favoring protonation and in turn catalyzing hydrogen production. Thus, an important question arose as to the impact of these non-CO moieties on dynamics and photochemistry. To address this, the solution-phase photochemistry of **18** was studied using time-resolved infrared spectroscopy in heptane, methanol, and acetonitrile.[65] It was observed that UV irradiation led to photolysis of a carbonyl ligand producing a tricarbonyl intermediate species. The population of this species was found to reduce on 100−200 ps timescales, assigned to recombination with CO ligands, but a bias towards a thermodynamically less stable isomeric form of the initial compound was noted. This suggested that facile interconversion of the ligand groups at the Fe center is possible in the unsaturated species. In a polar or hydrogen bonding solvent, this recombination-isomerization process was in competition with solvent substitution and formation of stable solvent adduct species was observed.

Later reports corroborated these findings and once again added data taken under longer wavelength excitation conditions. Work carried out in collaboration between the Stromberg, Webster and Heilweil groups demonstrated a small amount of variation in the photochemistry with excitation wavelength, in work focusing mainly on longer-term evolution of the signals.[66]

In addition to modification of the ligand composition of the sub-site analogue, it has been suggested that encapsulation of these molecules can be used to enhance catalytic function. To investigate the role of a matrix on photochemistry, the diphosphine species **1** was encapsulated in a low molecular weight (LMW) hydrogelator (Fmoc-Leu-Leu, Figure 17).[67] Combining infrared absorption with ultrafast

time-resolved infrared spectroscopy revealed significant contrasts in the chemical environment experienced by the encapsulated molecules. Furthermore, changes in the photochemistry were observed in comparison to the solution phase systems. Specifically, the gel provided a more rigid hydrogen bonding environment, restricting the isomerization following photolysis that was seen in solution. Of potential technological merit, the encapsulating matrix also imparted significant increases in stability of the sub-site analogue relative to a similarly aqueous solution. Since understanding and ultimately controlling the mechanistic role of ligands near Fe centers is likely to be crucial in exploiting artificial hydrogenases, it was suggested that these gels could offer a new option for future materials design involving catalysts.

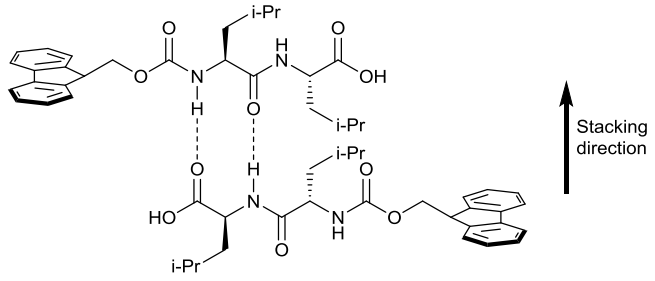

Figure 17. Fmoc-Leu-Leu hydrogelator.

Most recently, work has been carried out on the molecule **30** (Scheme 9). This followed exciting results showing that the molecule was able to catalyze the evolution of hydrogen gas without the need of the photosensitizer typically required for light driven H_2 production up to this point.[66,67] In an effort to understand the intimate details of the molecular mechanism leading to photo-hydrogen production we reported ultrafast UV_{pump}–IR_{probe} spectroscopy using three different excitation wavelengths and in a range of solvents, including under the conditions required for H_2 production.[70] Combining spectroscopic measurements of the photochemistry and vibrational relaxation dynamics with ground-state DFT calculations showed that, irrespective of experimental conditions, near-instantaneous carbonyl ligand loss is the main photochemical channel (Scheme 10). The initial study had been carried out using continuous wave excitation and it was proposed that a long-lived excited electronic state could be the basis for this functionality.[68,69] However, the additional time resolution of the new

experiments did not support this and pointed instead to a diffusive mechanism occurring in parallel with CO loss and recombination. This demonstrates the utility of ultrafast measurements in assisting in the extraction of underlying photochemical mechanisms operating during light-driven hydrogen generation.

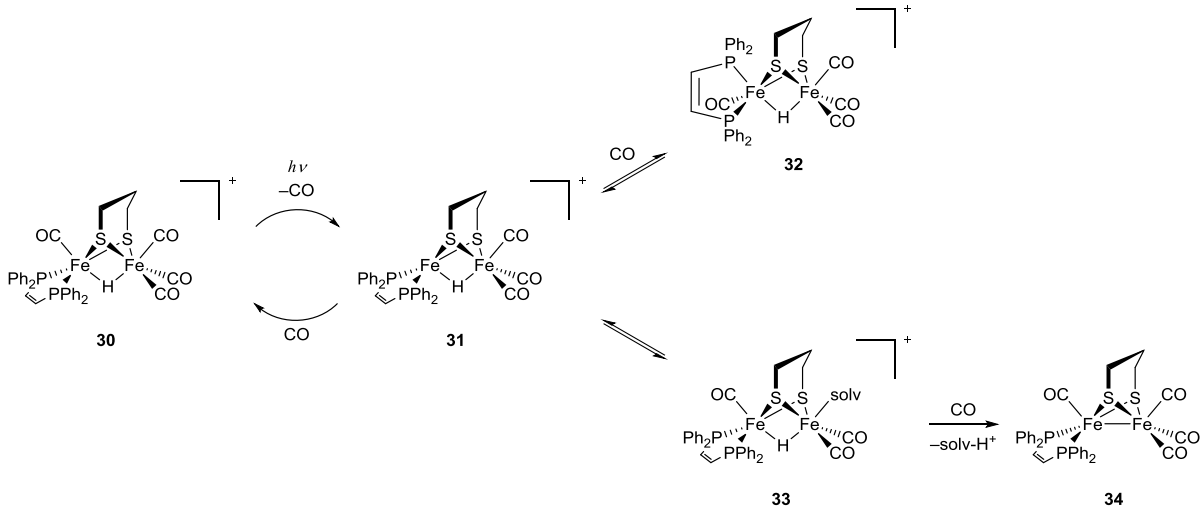

Scheme 10. Proposed mechanism of photochemistry observed by TRIR spectroscopy.[70]

The combination in this work of both excited state UV_{pump}-IR_{probe} and ground state IR_{pump}-IR_{probe} measurements revealed clear differences between the vibrational lifetime of the CO stretching modes (~50 ps) and the timescale for CO recombination (100−200 ps). This contrasts with recent reports linking dynamics on timescales of 100 ps observed following UV excitation of hydrogenase sub-site analogues with vibrational relaxation phenomena.[71] While some component of vibrational relaxation is widely acknowledged to contribute to UV_{pump}-IR_{probe} signals, a correlation such as that reported does not extend uniformly across all hydrogenase analogues studied so far and this assignment does not explain observed phenomena such as the recombination isomerization and diffusive photochemistry discussed above. It is however plausible that variations in individual experimental conditions may alter the balance between signals arising from ligand dissociation and vibrational relaxation following excitation.

Future directions

There remains the huge discrepancy between the activity of the natural system, with turnover number of 6000−9000 s^{-1} at potentials close to the reversible $2H^+/H_2$ couple,[24] and that of plausible models of the H-cluster or the subsite unit. The conformational flexibility of synthetic models limiting the accessibility of or the open 'rotated' state[72,73] and modulating the electronic condition of the subsite must in part be responsible for the slow catalysis. Simply put, the most catalytically-active conformer in the synthetic system is in low concentration within the array of states accessible to the molecule. In the enzyme, second -and third-coordination sphere interactions stabilize the active conformer and guide protons to the active site. It is essentially hydrogen-bonding interactions in the protein which establish the preferred conformational arrangement; controlling this in synthetic models by hydrogen bonding is a clear avenue for future work.

ACKNOWLEDGEMENTS

We gratefully acknowledge Dr Stephen Best (University of Melbourne), Dr Simon George (University of California, Irvine), Professor Luca De Gioia and Dr Maurizio Bruschi (both of the University of Milan-Bicocca), Professor Michael Hall (University of Texas, College Station) and Dr Saad Ibrahim (University of East Anglia) for their valuable contributions to the research summarized in the article together with the students and postdocs referenced herein who made this research possible. We thank the Biologic and Biotechnology Research Council (grant BB/E023290/1), Engineering and Physical Science Research Council (grants EP/M011879/1 and EP/D047943/1) and European Research Council (grant SPRITES-H2, ref. 334949) for funding the research.

References

1. Lubitz, W.; Ogata, H.; Rüdiger, O.; Reijerse, E. *Chem. Rev.* **2014**, *114*, 4081−4148.
2. Wright, J. A.; Pickett, C. J. In *Bioinspired Catalysis;* Weigand, W., Schollhammer, P., Eds.; Wiley-VCH, 2014, pp. 161−198.

3. Adamska, A.; Silakov, A.; Lambertz, C.; Rüdiger, O.; Happe, T.; Reijerse, E.; Lubitz, W. *Angew. Chem. Int. Ed.* **2012***, 51*, 11458−11462.
4. Tard, C.; Pickett, C. J. *Chem. Rev.* **2009***, 109*, 2245−2274.
5. Gloaguen, F.; Rauchfuss, T. B. *Chem. Soc. Rev.* **2009***, 38*, 100−108.
6. Simmons, T. R.; Berggren, G.; Bacchi, M.; Fontecave, M.; Artero, V. *Coord. Chem. Rev.* **2014***, 270−271*, 127−150.
7. Mulder, D. W.; Ratzloff, M. W.; Bruschi, M.; Greco, C.; Koonce, E.; Peters, J. W.; King, P. W. *J. Am. Chem. Soc*. **2014**, *136*, 15394−15402.
8. Stewart, A. I.; Clark, I. P.; Towrie, M.; Ibrahim, S.; Parker, A. W.; Pickett, C. J.; Hunt, N. T. *J .Phys. Chem. B* **2008**, *112*, 10023−10032.
9. Wright, J. A.; Pickett, C. J. *Chem. Commun.* **2009***, 45*, 5719−5721.
10. Jablonskytė, A.; Wright, J. A.; Pickett, C. J. *Dalton Trans.* **2010***, 39*, 3026−3034.
11. Razavet, M.; Borg, S. J.; George, S. J.; Best, S. P.; Fairhurst, S. A.; Pickett, C. J. *Chem. Commun.* **2002***, 36*, 700−701.
12. George, S. J.; Cui, Z.; Razavet, M.; Pickett, C. J. *Chem.—Eur. J.* **2002***, 8*, 4037−4046.
13. Jablonskytė, A.; Wright, J. A.; Fairhurst, S. A.; Peck, J. N. T.; Ibrahim, S. K.; Oganesyan, V. S.; Pickett, C. J. *J. Am. Chem. Soc.* **2011***, 133*, 18606−18609.
14. Zhao, X.; Georgakaki, I. P.; Miller, M. L.; Yarbrough, J. C.; Darensbourg, M. Y. *J. Am. Chem. Soc.* **2001***, 123*, 9710−9711.
15. Zaffaroni, R.; Rauchfuss, T. B.; Gray, D. L.; De Gioia, L.; Zampella, G. *J. Am. Chem. Soc.* **2012***, 134*, 19260−19269.
16. Ezzaher, S.; Capon, J.-F.; Gloaguen, F.; Pétillon, F. Y.; Schollhammer, P.; Talarmin, J. *Inorg. Chem.* **2007***, 46*, 3426−3428.
17. Justice, A. K.; Zampella, G.; De Gioia, L.; Rauchfuss, T. B. *Chem. Commun.* **2007***, 43*, 2019−2021.
18. Jablonskytė, A.; Wright, J. A.; Fairhurst, S. A.; Webster, L. R.; Pickett, C. J. *Angew. Chem. Int. Ed.* **2014***, 53*, 10143−10146.

19. Wright, J. A.; Webster, L.; Jablonskytė, A.; Woi, P. M.; Ibrahim, S. K.; Pickett, C. J. *Faraday Discuss.* **2011***, 148*, 359−371.
20. Van der Vlugt, J. I.; Rauchfuss, T. B.; Whaley, C. M.; Wilson, S. R. *J. Am. Chem. Soc.* **2005***, 127*, 16012−16013.
21. Jablonskytė, A.; Webster, L. R.; Simmons, T. R.; Wright, J. A.; Pickett, C. J. *J. Am. Chem. Soc.* **2014***, 136*, 13038−13044.
22. Liu, C.; Peck, J. N. T.; Wright, J. A.; Pickett, C. J.; Hall, M. B. *Eur. J. Inorg. Chem.* **2011**, 1080−1093.
23. Sarapu, A. C.; Fenske, R. F. *Inorg. Chem.* **1975**, *14*, 247–253.
24. Frey, M. *ChemBioChem* **2002**, *3*, 153−160.
25. Gloaguen, F.; Lawrence, J. D.; Rauchfuss, T. B. *J. Am. Chem. Soc.* **2001**, *123*, 9476−9477.
26. Le Cloirec, A.; Best, S. P.; Borg, S.; Davies, S. C.; Evans, D. J.; Hughes, D. L.; Pickett, C. J. *Chem. Commun.* **1999**, *35*, 2285−2286.
27. Eilers, G.; Schwartz, L.; Stein, M.; Zampella, G.; de Gioia, L.; Ott, S.; Lomoth, R. *Chem.—Eur. J.* **2007**, *13*, 7075−7084.
28. Lyon, E. J.; Georgakaki, I. P.; Reibenspies, J. H.; Darensbourg, M. Y. *J. Am. Chem. Soc.* **2001**, *123*, 3268−3278.
29. Li, B.; Liu, T.; Singleton, M. L.; Darensbourg, M. Y. *Inorg. Chem.* **2009**, *48*, 8393−8403.
30. Tard, C.; Liu, X.; Ibrahim, S. K.; De Gioia, L.; Davies, S. C.; Yang, X.; Wang, L.-S.; Sawers, G.; Pickett, C. J. *Nature* **2005**, *433*, 610−613.
31. Camara, J. M.; Rauchfuss, T. B. *J. Am. Chem. Soc.* **2011**, *133*, 8098−8101.
32. Camara, J. M.; Rauchfuss, T. B. *Nat. Chem.* **2012**, *4*, 26−30.
33. Wright, J. A.; Pickett, C. J. *ChemCatChem* **2012**, *4*, 1723−1724.
34. Erdem, Ö. F.; Schwartz, L.; Stein, M.; Silakov, A.; Kaur-Ghymaan, S.; Huang, P.; Ott, S.; Reijerse, E. J.; Lubitz, W. *Angew. Chem. Int. Ed*. **2011**, *50*, 1439−1443.
35. Liu, T.; Darensbourg, M. Y. *J. Am. Chem. Soc.* **2007**, *129*, 7008−7009.

36. Justice, A. K.; Rauchfuss, T. B.; Wilson, S. R. *Angew. Chem. Int. Ed.* **2007**, *46*, 6152−6154.
37. Borg, S.; Behrsing, T.; Best, S. P.; Razavet, M.; Liu, X.; Pickett, C. J. *J. Am. Chem. Soc.* **2004**, *126*, 16988−16999.
38. Aguirre de Carcer, I.; DiPasquale, A.; Rheingold, A. L.; Heinekey, D. M. *Inorg. Chem.* **2006**, *45*, 8000−8002.
39. Tard, C.; Liu, X.; Hughes, D. L.; Pickett, C. J. *Chem. Commun.* **2005**, *41*, 133−135.
40. Cheah, M. H.; Tard, C.; Borg, S. J.; Liu, X.; Ibrahim, S. K.; Pickett, C. J.; Best, S. P. *J. Am. Chem. Soc*. **2007**, *129*, 11085−11092.
41. Borg, S. J.; Tye, J. W.; Hall, M. B.; Best, S. P. *Inorg. Chem.* **2007**, *46*, 384−394.
42. Surawatanawong, P.; Hall, M. B. *Inorg. Chem.* **2010**, *49*, 5737−5747.
43. Wang, W.; Nilges, M. J.; Rauchfuss, T. B.; Stein, M. *J. Am. Chem. Soc.* **2013**, *135*, 3633−3639.
44. Wang, W.; Rauchfuss, T. B.; Zhu, L.; Zampella, G. *J. Am. Chem. Soc.* **2014**, *136*, 5773−5782.
45. Kaziannis, S.; Wright, J. A.; Candalaresi, M.; Kania, R.; Greetham, G. M.; Parker, A. W.; Pickett, C. J.; Hunt, N. T. *PhysChemChemPhys* **2011**, *13*, 10295−10305.
46. Bonner, G. M.; Ridley, A. R.; Ibrahim, S. K.; Pickett, C. J.; Hunt, N. T. *Faraday Discuss.* **2010**, *145*, 429−442.
47. Ridley, A. R.; Stewart, A. I.; Adamczyk, K.; Ghosh, H. N.; Kerkeni, B.; Guo, Z. X.; Nibbering, E. T. J.; Pickett, C. J.; Hunt, N. T. *Inorg. Chem.* **2008**, *47*, 7453−7455.
48. Dougherty, T. P.; Grubbs, W. T.; Heilweil, E. J. *J. Phys. Chem.* **1994**, *98*, 9396−9399.
49. George, M. W.; Dougherty, T. P.; Heilweil, E. J. *J. Phys. Chem.* **1996**, *100*, 201−206.
50. Kempner, W.; Kubowitz, F. *Biochem. Z.* **1933**, *265*, 245−252.
51. Thauer, R. K.; Kaufer, B.; Zahringe. M; Jungerma. K *Eur. J. Biochem.* **1974**, *42*, 447−452.
52. Patil, D. S.; Czechowski, M. H.; Huynh, B. H.; Legall, J.; Peck, H. D.; Dervartanian, D. V. *Biochem. Biophys. Res. Commun.* **1986**, *137*, 1086−1093.
53. Patil, D. S.; Huynh, B. H.; He, S. H.; Peck, H. D.; Dervartanian, D. V.; Legall, J. *J. Am. Chem. Soc.* **1988**, *110*, 8533−8534.

54. Kowal, A. T.; Adams, M. W. W.; Johnson, M. K. *J. Biol. Chem.* **1989**, *264*, 4342−4348.

55. Lemon, B. J.; Peters, J. W. *Biochemistry* **1999**, *38*, 12969−12973.

56. De Lacey, A. L.; Stadler, C.; Cavazza, C.; Hatchikian, E. C.; Fernandez, V. M. *J. Am. Chem. Soc.* **2000**, *122*, 11232−11233.

57. Lemon, B. J.; Peters, J. W. *J. Am. Chem. Soc.* **2000**, *122*, 3793−3794.

58. Chen, Z. J.; Lemon, B. J.; Huang, S.; Swartz, D. J.; Peters, J. W.; Bagley, K. A. *Biochemistry* **2002**, *41*, 2036−2043.

59. Parkin, A.; Cavazza, C.; Fontecilla-Camps, J. C.; Armstrong, F. A. *J. Am. Chem. Soc.* **2006**, *128*, 16808−19815.

60. Goldet, G.; Brandmayr, C.; Stripp, S. T.; Happe, T.; Cavazza, C.; Fontecilla-Camps, J. C.; Armstrong, F. A. *J. Am. Chem. Soc.* **2009**, *131*, 14979−14989.

61. Roseboom, W.; De Lacey, A. L.; Fernandez, V. M.; Hatchikian, E. C.; Albracht, S. P. J *J. Biol. Inorg. Chem.* **2006**, *11*, 102−118.

62. Kaziannis, S.; Santabarbara, S.; Wright, J. A.; Greetham, G. M.; Towrie, M.; Parker, A. W.; Pickett, C. J.; Hunt, N. T. *J. Phys. Chem. B* **2010**, *114*, 15370−15379.

63. Bingaman, J. L.; Kohnhorst, C. L.; Van Meter, G. A.; McElroy, B. A.; Rakowski, E. A.; Caplins, B. W.; Gutowski, T. A.; Stromberg, C. J.; Webster, C. E.; Heilweil, E. J. *J. Phys. Chem. A* **2012**, *116*, 7261−7271.

64. Stewart, A. I.; Wright, J. A.; Greetham, G. M.; Kaziannis, S.; Santabarbara, S.; Towrie, M.; Parker, A. W.; Pickett, C. J.; Hunt, N. T. *Inorg. Chem.* **2010**, *49*, 9563−9573.

65. Kania, R.; Frederix, P. W. J. M.; Wright, J. A.; Ulijn, R. V.; Pickett, C. J.; Hunt, N. T. *J. Chem. Phys.* **2012**, *136*, 044521.

66. Johnson, M.; Thuman, J.; Letterman, R. G.; Stromberg, C. J.; Webster, C. E.; Heilweil, E. J. *J. Phys. Chem. B* **2013**, *117*, 15792−15803.

67. Frederix, P. W. J. M.; Kania, R.; Wright, J. A.; Lamprou, D. A.; Ulijn, R. V.; Pickett, C. J.; Hunt, N. T. *Dalton Trans.* **2012**, *41*, 13112−13119.

68. Bertini, L.; Fantucci, P.; De Gioia, L.; Zampella, G. *Inorg. Chem.* **2013**, *52*, 9826−9841.
69. Wang, W.; Rauchfuss, T. B.; Bertini, L.; Zampella, G. *J. Am. Chem. Soc.* **2012**, *134*, 4525−4528.
70. Frederix, P. W. J. M.; Adamczyk, K.; Wright, J. A.; Tuttle, T.; Ulijn, R. V.; Pickett, C. J.; Hunt, N. T. *Organometallics* **2014**, *33*, 5888−5896.
71. Caplins, B. W.; Lomont, J. P.; Nguyen, S. C.; Harris, C. B. *J. Phys. Chem. A* **2014**, *118*, 11529−11540.
72. Nicolet, Y.; de Lacey, A. L.; Vernède, X.; Fernandez, V. M.; Hatchikian, E. C.; Fontecilla-Camps, J. C. *J. Am. Chem. Soc.* **2001***, 138*, 1596−1601.
73. Darensbourg, M. Y.; Lyon, E. J.; Zhao, X.; Georgakaki, I. P. *Proc. Natl. Acad. Sci. USA* **2003**, *100*, 3683−3688.

TOC Graphic

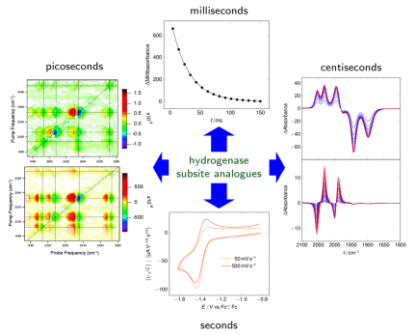

TOC Entry

Time-resolved techniques in the elucidation of photon, proton and electron-transfer reactions of synthetic analogues of the subsite of FeFe-hydrogenase are discussed.